The International Journal of Advanced Manufacturing Technology (2022) 119:2445–2460
https://doi.org/10.1007/s00170-021-08106-y

ORIGINAL ARTICLE

Influence of the manufacturing parameters of an AlMg5 wire–based hybrid production process on quality and mechanical properties

Hans-Christian Möhring[1] · Dina Becker[1] · Rocco Eisseler[1] · Thomas Stehle[1] · Tim Reeber[1]

Received: 29 May 2021 / Accepted: 18 September 2021 / Published online: 15 December 2021

Abstract
Hybrid manufacturing processes are known for combining the advantages of additive manufacturing and more traditional manufacturing processes such as machining to create components of complex geometry while minimising material waste. The trend towards lightweight design, especially in view of e-mobility, gives aluminium materials an important role to play. This study examines the use of aluminium alloys in laser metal wire deposition (LMWD) processes with subsequent subtractive machining, which is considerably more difficult due to the different process-related influences. The investigations are focussed on the influence of the differently controlled laser power on the shape accuracy, the microstructure, and the hardness of the AlMg5 test components after the LMWD process with subsequent subtractive machining by turning. The long-term goal of the investigations is to increase the stability of the hybrid production process of AlMg5 components with defined dimensional accuracy and mechanical properties.

Keywords Additive-subtractive manufacturing · Laser metal deposition · AM post-processing · Machining · Accuracy · Microstructure · Hardness

1 Introduction

Due to their suitability for lightweight design, aluminium components are widely used in many areas such as the automotive and aerospace industries. The production of aluminium components using casting technology is expensive and environmentally harmful due to the production of the casting moulds and the high energy and material costs [1–5]. The machining of aluminium components usually involves a high machining volume, which in principle offers an approach for optimization. With generative manufacturing processes, these problems do not arise as the aluminium components can be directly produced without forming tools and close to the final contour [6–8]. However, generative manufacturing processes are not yet capable of producing dimensionally accurate components on their own [9]. Especially surfaces of which the shape and surface quality are decisive for the later sub-functions of the component (such as surfaces for bearings or for interlocking connections) must be machined after the printing process. To combine the advantages of additive and subtractive processes, so-called hybrid machining centres are becoming increasingly popular, which can guarantee a complete additive-subtractive design process in one clamping, thus increasing the accuracy of the process. Currently, only additive processes, which fall under the category of direct energy deposition (DED), are taken into consideration for such hybrid centres. DED processes can use powder or wire as application material, and, in contrast to the equally popular powder bed processes, they generally have higher deposition rates (especially when using wire), which lead to shorter design times [10]. This is achieved through a higher laser power and a greater wire feed, which in turn result in a greater layer thickness. At the same time, DED processes have a poorer surface quality and lower dimensional accuracy, which leads to a higher volume to be machined [11–16].

To keep the volume to be machined low, it is necessary to make the deposition process itself more dimensionally stable and to improve the surface quality resulting from the additive process. In the deposition process, the implementation of these requirements is determined by the occurring molten pool. The characteristics of the molten pool are

✉ Dina Becker
dina.becker@ifw.uni-stuttgart.de

[1] Institute for Machine Tools (IfW), University of Stuttgart, Holzgartenstraße 17, 70174 Stuttgart, Germany

decisively influenced by the laser power and thus by the power absorbed in the material.

One of these DED processes that uses wire as filler material is laser metal wire deposition (LMWD). In LMWD, wire is continuously applied in layers to the substrate via a nozzle [17, 18]. Analogously to powder-based processes, the applied molten material is shielded by a protective gas to suppress the danger of possible reactions (primarily oxidation) [19, 20].

This study examines the influence of a laser power control during the laser cladding process on the quality of the test components as well as the influence of subsequent machining. The test components produced by the laser cladding process were evaluated based on form accuracy, surface roughness, microstructure, and hardness before and after subtractive machining.

2 Test components und process setup

2.1 LMWD with a closed loop control of the track height

The additively manufactured components (cylinders) were produced at the Institut für Strahlwerkzeuge (IFSW), University of Stuttgart [21]. A picture from the processing head and schematics and a picture of the process itself and can be seen in Fig. 1.

LMWD uses laser radiation to melt the filler material as well as the substrate to generate tracks similarly to a welding process. The laser radiation is absorbed by the base material or the already deposited tracks, and the increase in temperature forms a melt pool. The wire is fed into the process zone coaxially, as shown in Fig. 1. Through the deposition of multiple tracks, a three-dimensional part can be generated.

For the generation of the cylindrical samples, the processing head follows a helical path. In previous works, an accumulation of heat from the continuous absorption of laser radiation in the generation of the samples was observed [21]. Due to a changing heat convection (good near the build plate, increasingly worse with increasing height), the heat accumulates, and the melt pool widens. This leads to deviations of the height and the diameter of the cylinders and even to a collapse of the process since the focus of the laser is fixed in relation to the programmed track. The programmed deposition heights are not met as planned due to the melt pool widening, the laser melts the filler material mid-air away from the melt pool, and the process stops.

In addition, the deposited tracks show local deviations of the track height, which accumulate to an uneven upper side of the cylinder. To combat this, a coaxial OCT (optical coherence tomography) was installed to measure the distance to the upper side of the cylinder. These measurements are the basis for a closed loop control of the wire feed rate. While it would have also been possible to choose the track feed rate, the wire feed rate possesses a higher dynamic. If the track height is insufficient, the OCT-based closed loop control increases the wire feed rate to compensate for the local deviations. To avoid melt pool widening, the laser power was decreased manually to avoid overheating. A pyrometer signal was used as reference [21]. With the

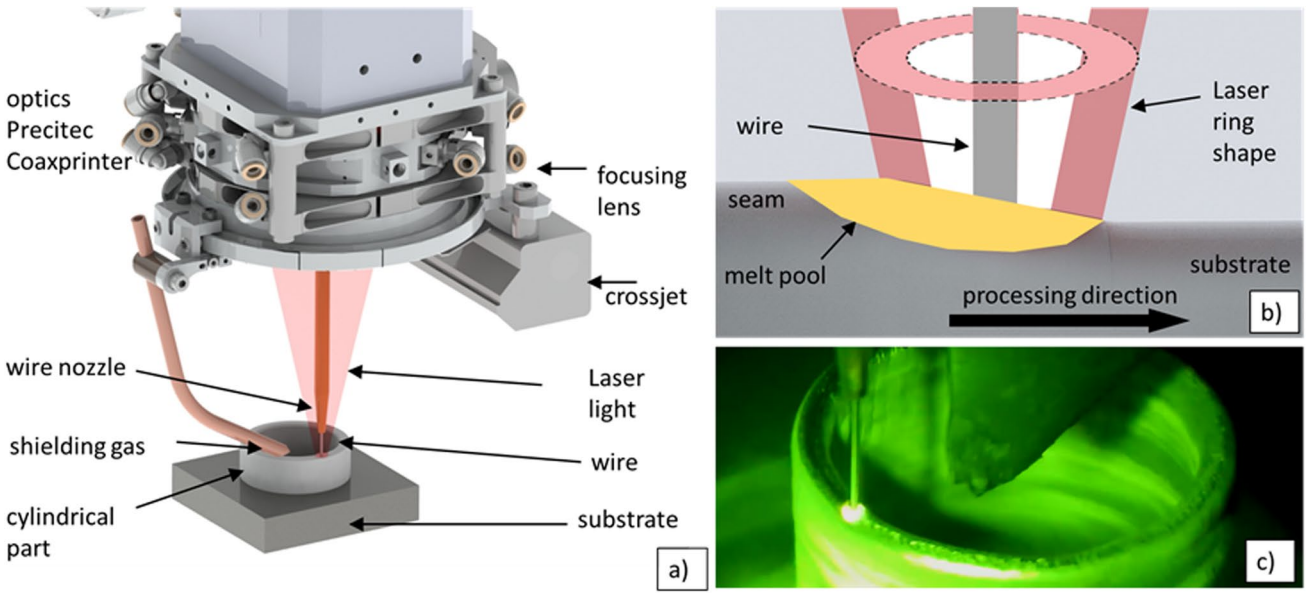

Fig. 1 LMWD-process: **a** processing head; **b** laser ring shape and wire; **c** deposition process [21]

Table 1 Parameters of the sample-production using the LMWD-process with an OCT-based height control

Laser power	2640–1200 W (varied)
Fibre diameter	600 µm
Wavelength	1030 nm
Track speed	2 m/min
Wire speed	4 m/min
Beam diameter	2–3 mm
Shielding gas	Nitrogen (20 l/min)
Programmed cylinder height	37 mm
Programmed cylinder diameter	37 mm
Wire diameter	1 mm
Wire material	AlMg5 (5356)
Substrate material	AlSi1MgMn (6082)

decrease in laser power, the input of heat into the process is decreased. In doing so, the melt pool will stop widening.

Table 1 shows the parameters of the production process using the LMWD-process with an OCT-based height control. The laser power was varied from 2640 to 1450 W. This was necessary to counteract overheating of the components during the process. The accumulation of heat in the upper part of the cylindrical components due to deteriorating heat conduction contributed to the premature termination of the process at constant laser power values. Therefore, it is essential to control the power to lower power values during component production to ensure the completion of the process. Wire feed rate, focal point position, process gas type, and process gas quantity were kept constant.

As filler material, AlMg5 wire with a diameter of $d = 1$ mm was used which is also used in standard MIG/MAG welding applications. AlMg5 is a 5356-type aluminium solid TlG welding material and suited for use with Ar or Ar + He mixed shielding gases. AlMg5 is capable of welding Al–Mg alloys, Al–Mg-Zn alloys, dissimilar aluminium alloy grades containing up to 5% Mg as well as components which are subsequently to be anodised.

The development of the controlled LMWD process was conducted by the IFSW (University of Stuttgart) [21]. The work presented here is focused on the quality analysis of the additively manufactured specimens before and after machining. Due to the novelty of the process, the OCT-based height tracking should enable automatic control of the laser power in the future. The study presents a practical elaboration of the process with three variants of manual reduction of the laser power for the subsequent process configuration of the LMWD process. One of the objectives in LMWD-process was to fabricate the homogeneous thin-walled test parts in LMWD process. To determine the optimum parameters for manufacturing the cylinders, it was necessary to reduce the laser power to avoid heat build-up due to continuous heat input to the workpiece. Three LMWD processes were tested using OCT control. For process A, the laser power was mainly reduced in two steps ($h = 9.44$–11.7 mm; $h = 17.6$ mm), for process B, relatively continuously, and for process C in two steps in process start and six more ($h = 14.8$–16.8 mm) over the part height.

The work presented here is focused on the quality analysis of the additively manufactured specimens before and after machining. Accordingly, the examined test components were classified into group A (laser power A), group B (laser power B), and group C (laser power C).

2.2 Machining setup

To produce the desired cylindrical nominal contour on the additively manufactured samples, these were subsequently machined. The required external and internal longitudinal turning was carried out on an R200 turning/milling centre from INDEX-Werke GmbH & Co. KG. using water-based flood cooling lubrication (Blasocut BC 935 K). In Fig. 2, the machining setup as well as the used tools can be seen. For the external and the internal turning process, carbide inserts with a radius of 0.4 mm were used. The cutting parameters were varied within the sample: In the lower area near the build plate, the effects of a feed rate of $f_1 = 0.05$ mm/revolution were investigated, whereas in the upper area of the samples a feed rate of $f_2 = 0.1$ mm/revolution was used (internal as well as external). For reference, the middle area of the samples was not machined. In all cases, the cutting velocity was kept constant at $v_c = 500$ m/min. The machining parameters were taken from [22].

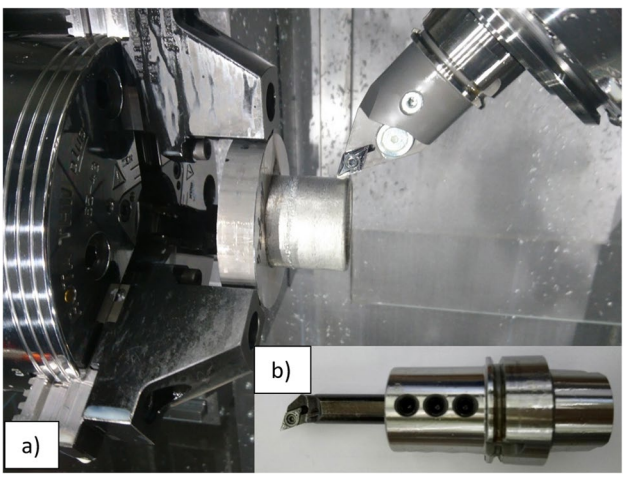

Fig. 2 **a** External turning process; **b** tool used for internal turning

3 Measurement setups

3.1 Dimensional accuracy

The additively manufactured cylindrical part was analysed using a 3D coordinate measuring machine of type MC850 from Carl Zeiss AG using an Ultra High Precision Caliper probe system with a measuring ball radius of 2.5 mm. The measuring strategy for the samples was created with the software "Calypso" to measure the element from the outside and inside with a tactile probe. The measuring distance along the additive build direction (*Z*-axis) was 1 mm. Thus, several inner and outer diameters of the samples were measured with an accuracy of 0.1% relative deviation. The roundness (deviation from the geometrically perfect circle) was determined according to DIN ISO 2768–2.

3.2 Metallographic studies

To determine the macroscopic structure of the samples, the samples were subjected to etching with caustic soda solution. For this purpose, the samples were carefully separated with a cut-off wheel with interrupted cuts, embedded, ground (grain size 240, 500, 1000, 2000, and 4000, pressure force 20–30 N) and then polished with a diamond suspension (ATM Dia-COMPLETE Poly 9 µm, 3 µm, and 0.25 µm) on a synthetic fibre plate (3 µm). The macro etching was achieved by immersing the samples in a 10% NaOH solution heated to approx. 55 °C.

The electrolytic etching process of Barker enables the creation of colour etchings in aluminium alloys. The etching influences the individual grains of the structure depending on their orientation. The investigated samples were embedded using a 2-component embedding agent based on highly cross-linked methyl methacrylate, grinded up to a 4000-grain in size steps 320, 500, 800, 1000, 2500, and 4000, then polished with diamond suspension on a synthetic fibre plate (3 µm). Electrolytic colour etching was performed with a Struers LectroPol-5 with a 5-cm^2 aperture, at a voltage of 16 V and a flow rate of 10 l/min. The electrolyte used was a 50% borofluoric acid at 20 °C for 90 s. The samples were then examined under a polarisation microscope.

3.3 Mechanical properties

To determine the hardness, the instrumented indentation test was carried out according to DIN EN ISO 14577–1 and ASTM E 2546 using a Picodentor HM500. In this method, the applied force and the penetration depth are continuously measured during the loading and unloading phase. The Martens hardness (HM) is defined as the ratio of the maximum force to the corresponding contact area and is given in the unit N/mm^2. Unlike the Vickers or Brinell method, the hardness value is determined from plastic and elastic deformation. The hardness test was carried out under the conditions listed in Table 2.

4 Results and discussion

In this chapter, the produced samples are evaluated after the additive process and after the machining process. For both processes, metallographic studies as well as hardness investigations are presented.

4.1 Influence of the laser control on the shape accuracy of the additive process

As already described in Chapter 2, the test components were manufactured under decreasing laser power levels to ensure a stable and complete process. This was done to counteract the overheating of the part, since the heat convection of the process was not sufficient to work with a constant laser power. Overheating resulted in failed processes since melt pool widening increased to fatal levels. Then the focus of the laser lost contact with the part, and the wire was melted in mid-air [21].

In all tests, the LMWD process was started with a high laser power of 2400–2600 W and finished with a laser power of 1200–1400 W. Since the laser power was adjusted manually by visual inspection and with a knob, it was inevitable that the desired laser power was oversteered. This resulted in short drops in laser power, which were compensated immediately by the process engineer. During the process, the laser power was reduced twice in group A: from 2640 to 1620 W (between 9.44 and 11.7 mm) and from 1620 to 1440 W (at 17.6 mm). For group B, there was a continuous reduction of the laser power from 2640 to 1800 W in the range between 1 and 9 mm and a further three-stage reduction to 1400 W in the range between 16 and 24 mm. For group C, the laser power was reduced in two steps from 2520 to 2280 W (component height 1 to 5 mm) at the beginning of the process and in six steps from 2280 to 1440 W (component height 14.8–17.2 mm).

Figure 3 shows the laser power curves during the manufacturing processes of the examined components.

Table 2 Measurement parameters of the hardness evaluation

Measurement force	400 mN
Duration loading phase	5 s
Duration holding phase	10 s
Duration unloading phase	5 s

In the visual analysis of the manufactured test components, as shown in Fig. 4, differences in the surface finish could easily be detected. The cylinder test groups A and C showed clear transition marks around the strong laser power reduction. In contrast, the soft continuous reduction of the laser power during the production of group B did not leave any noticeable marks on the cylinder surface (group C).

The control of the laser power significantly influences the wall thickness of the manufactured cylinders. Figure 5 illustrates the radii of the investigated samples obtained by tactile measurement. After the strong reduction in laser power for the samples A (11 mm) and C (18 mm), the wall thickness decreased during the following 1.5–2.0 mm and then increased due to the high temperature gradients in the

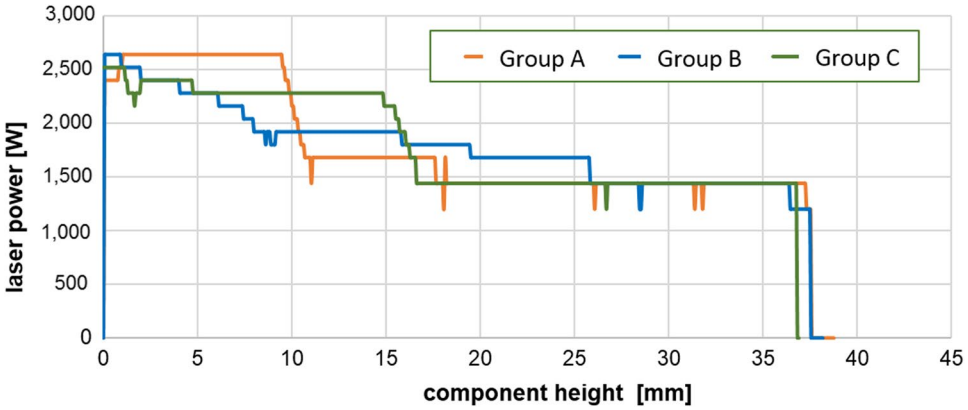

Fig. 3 Laser power during the LMWD process

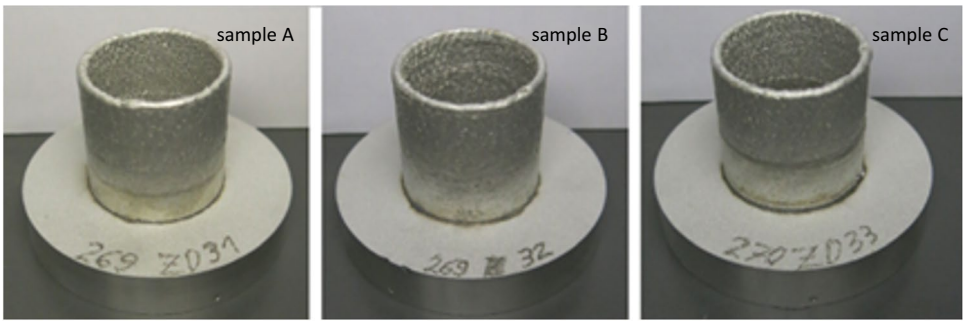

Fig. 4 LMWD manufactured test components of group A, B, and C: selected sample A, sample B, and sample C

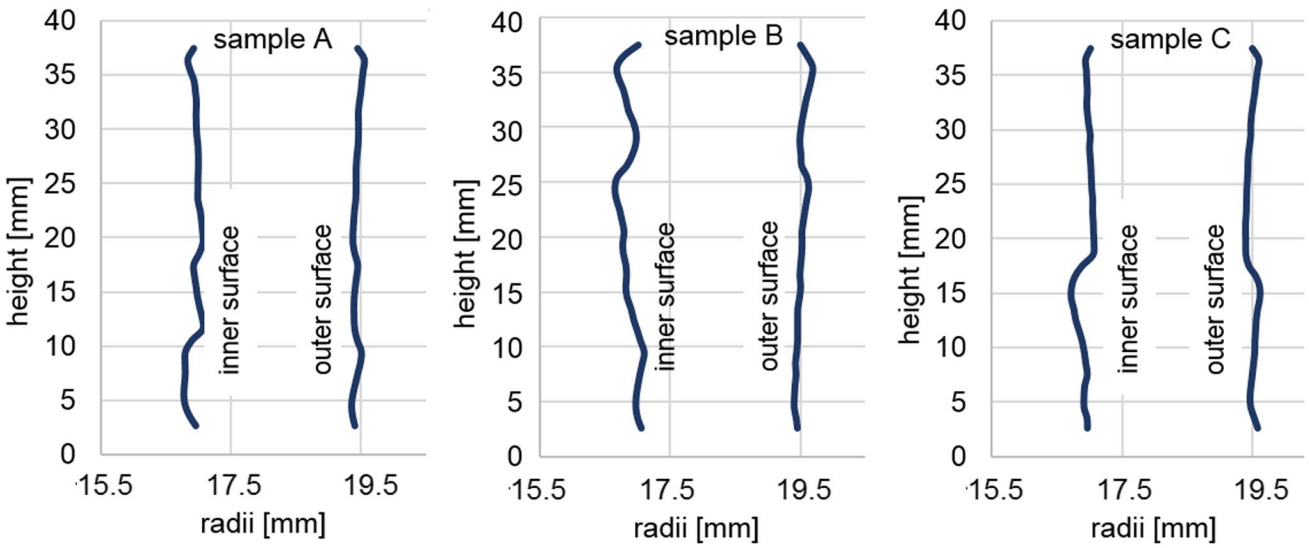

Fig. 5 Laser control influence on the wall thickness: sample A, sample B, and sample C

molten bath, which caused a widening of the molten bath. This was the same effect that causes the sample production to fail at constant laser power parameters, but this effect is constrained due to the reduction in laser power. For sample B, the minimum wall thickness was measured at 9 mm after the first small power adjustment and at 28.5 mm after the last control stage, which illustrated the process-stabilising influence of the laser control. It should also be noted that all the components examined offer a better straightness at the outer cylinder side than at the inner one. These differences could be explained by the specific heat conduction in the partially closed space of the additive-manufactured component, which resulted in thermally induced tensions. The heat dissipation was more advantageous on the outside than on the inside because the environment helped to dissipate the heat on the outside, whereas the heat built up on the inside. This had a negative effect on the shape (straightness) of the component [16].

In addition to the wall thickness, the laser power also had a significant effect on the roundness of the cylinders. A particularly negative effect was caused by the short and abrupt changes in laser power, which could be explained by a short drop in laser power due to manual adjustment. In the 1.6–2.5 mm range (sample C), the laser power fell from 2520 to 2160 W and then rose again to 2400 W. This resulted in a roundness value of 0.6 mm on the outer and 0.3 mm on the inner side of the component (Fig. 6). In comparison, the roundness changed from 0.17 to 0.23 mm (outside) and from 0.29 to 0.32 mm (inside), when a much greater, step-like reduction in laser power from 2280 to 1440 W took place in the 14.8–16.8 mm range for sample B. Similarly, strong fluctuations in roundness were observed, when the laser power oscillated around a target power value for the sample A (11.5 mm and 17 mm cylinder height). It should be noted that this oscillation had a much greater effect on the roundness of the outer sides of the cylinder than on the inner side. In the area of continuous (stepwise) reduction or constant laser power, the roundness on the outer cylinder wall was generally better (smaller roundness values) than on the inner one. The increased roundness values could be attributed to the last layer, which formed quite irregularly compared to the other layers. The highest temperature gradients occurred in the top region, which resulted in high values of stress. The confining stress relief led to strong dimensional deviations. These deviations should be post-processed together with the deviations over the component wall.

4.2 Influence of subtractive machining

To increase the dimensional accuracy of the test components, the components were turned from the outside and inside, as shown in Fig. 7. The depth of cut was 0.3 mm (calculated starting from r_{min} on the outside and from r_{max} on the inside). The removed metal amounted to 14% (group A and group B) and 20% (group C) of the complete material volume. The feed rate f_1 was used in the lower area, whereas the feed rate f_2 was used in the upper part. In the lower range (f=0.05 mm/rev), it was examined how the laser power influences the mechanical properties (hardness) of the components. In the upper range (f=0.1 mm/rev), it was analysed how the hardness is influenced by the amount of the material to be removed with the same laser power (see 4.4).

Figure 8 shows the roundness of the test components on both wall sides of the cylinders before and after turning. It could be clearly seen that all the components tested showed good roundness values of max. 0.029 mm after machining (max. 0.38 mm before machining). The difference in roundness values (mean value) on the outer and inner side of the machined test components was max. 0.019 mm for f_1 (sample A) and max. 0.005 mm for f_2 (sample C). Regarding

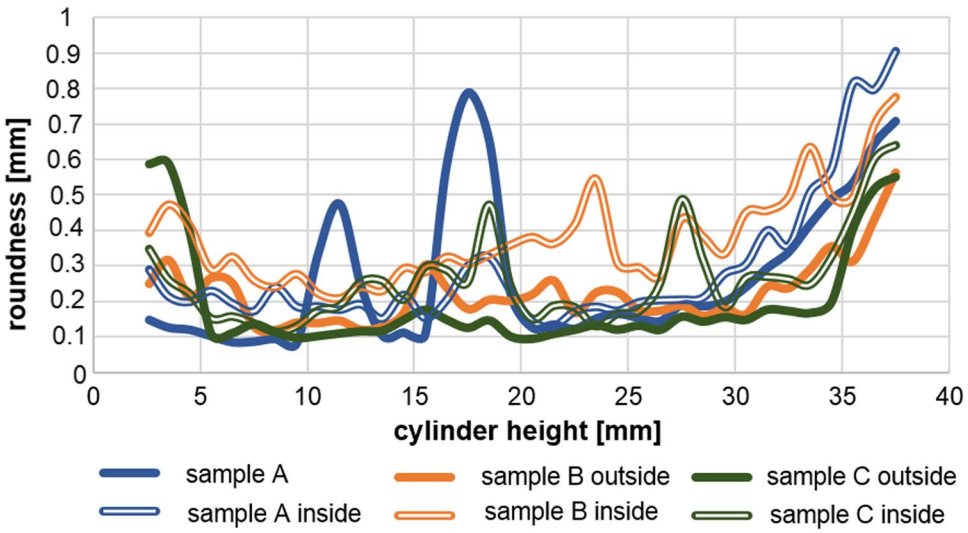

Fig. 6 Roundness of the samples along their height

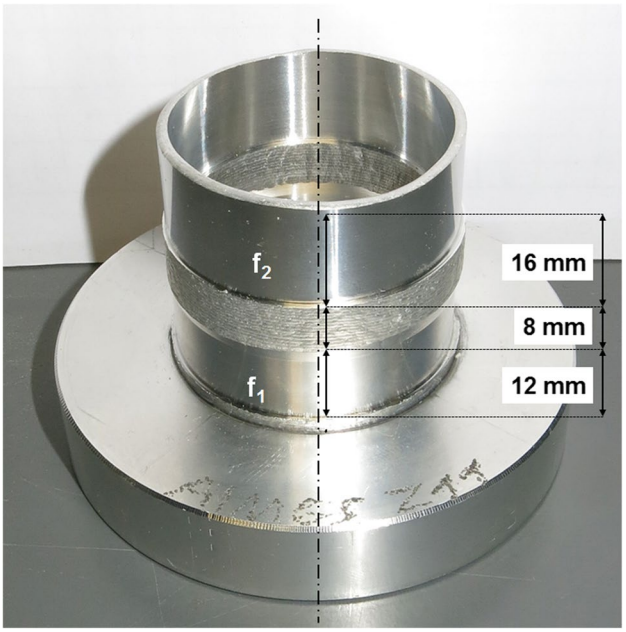

Fig. 7 Sample after turning. The original surface in the middle was preserved to have a reference to post AM conditions

the partial areas without machining, this difference reached max. 0.212 mm (sample A pre-machining area f_1), 0.225 mm (sample B pre-machining area f_2) and 0.18 mm (sample C pre-machining area f_2). Thus, it could be concluded that a high shape accuracy with a deviation of max. 0.02 mm from the geometrically perfect circle was achieved over the entire wall thickness of the additive-subtractive test components, when using the machining parameters of the turning process. The roundness of all machined components here differed minimally. Components that were machined with higher feed rates tend to have slightly lower roundness values. This could be explained by higher machining forces and temperatures when machining at higher feed rates. This favoured plastic deformation on the component wall, and surface defects (pores) could be "repaired" in a better way.

4.3 Results of the metallographic studies

After the roundness was determined, the cylinders were cut off at 4 mm height from the building platform, carefully separated in their centre and prepared for the metallographic examinations. This is intended to make the layer transitions within the component more visible. First, the samples were parted while avoiding the induction of heat into the component. After enclosure, they were grinded, polished, and etched with NaOH like mentioned in chapter 3.2.

The prepared sections of investigated samples were examined macroscopically and compared with each other. The results are represented in Fig. 9. It was found that the largest layer heights fall into the areas of laser power reduction. If the laser power is reduced during the 9.44–11.03 mm cylinder height, this results in three wider layers (sample A/area a). A further jump in layer height can be observed at 17.5–18.3 mm of cylinder height (sample A/area b), where the laser power was reduced from 1680 to 1440 W during the deposition process. Similar correlations between the layer thickness and the laser power were found for sample B/area a and sample C/area a. This probably correlates with the

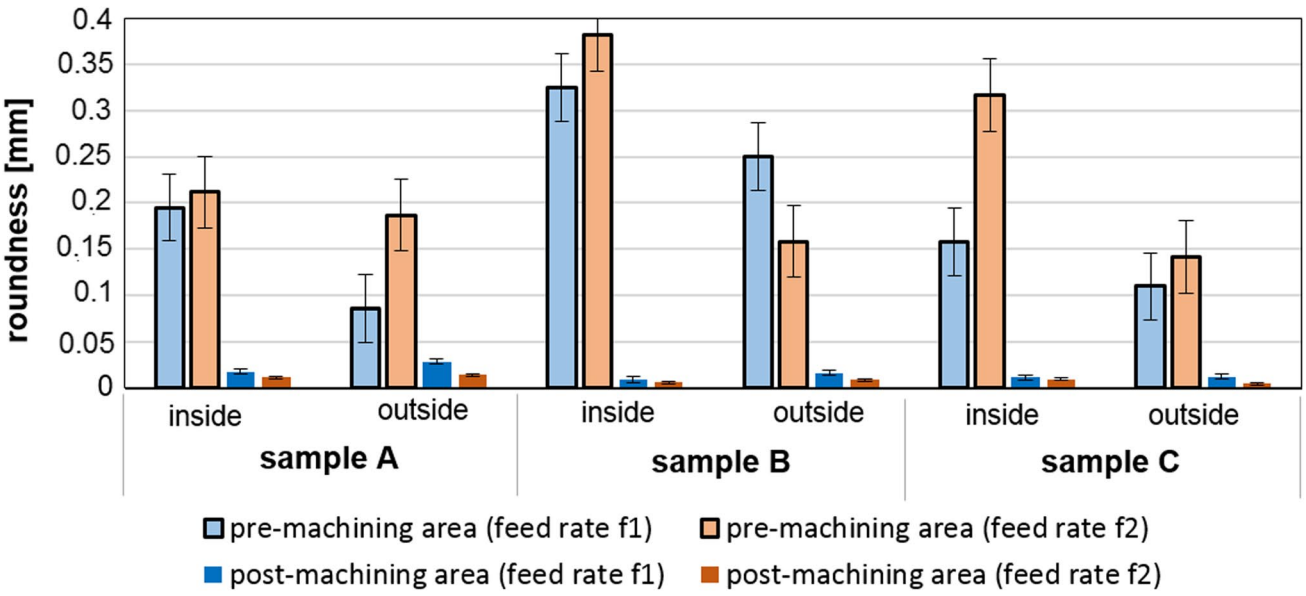

Fig. 8 Roundness of the samples in the post-additive and post-machining areas, examined in the areas of feed rate f_1 and f_2

reduction of the laser power and an increased wire feed from the wire feed control loop. This compensated for inequalities (dips, which were registered by the OCT) in the cylinder face in the process.

Overall, the average layer height of the manufactured test components up to the top layer was between 500.56 and 513.03 µm. Table 3 shows an evaluation of the layer heights. The uppermost layer has a layer height value that is approx. 2.7–2.9 times higher than the other built-up layers.

To determine the change in the microstructure after the additive process, sections of the AlMg5 wire were first examined. Etchings can be seen in Fig. 10. The longitudinal section shows a strongly stretched and anisotropic structure of the wire structure, which is produced during the production of the wire (wire forming). The cross section shows an isotropic globulistic microstructure of the wire with irregularly distributed gas pores and microblowholes, which are formed during hydrogen precipitation during the solidification of the wrought Al alloys and were described in detail by Kostron and Lutze [23, 24]. The cuts were also used to obtain comparative hardness measurements of the base material. The hardness in the longitudinal sections was

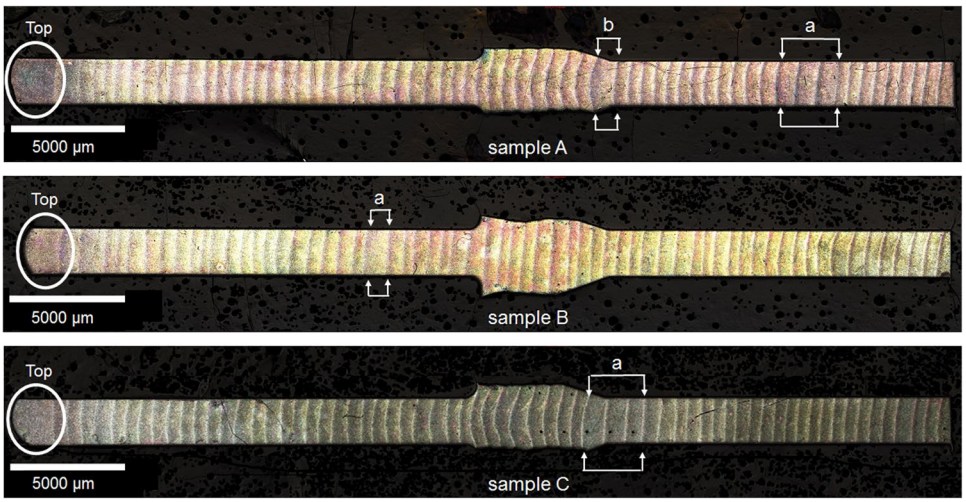

Fig. 9 Etchings of samples A, B, and C (NaOH-etching)

Table 3 Layer heights of the test components

Test component	Layer height without upmost layer (averaged) [µm]	Maximal layer height without upmost layer [µm]	Minimal layer height without upmost layer [µm]	Height of the upmost layer [µm]
Sample A	513.03	802.11	355.23	1420.49
Sample B	503.49	852.78	303.56	1326.01
Sample C	500.56	789.04	328.98	1418.06

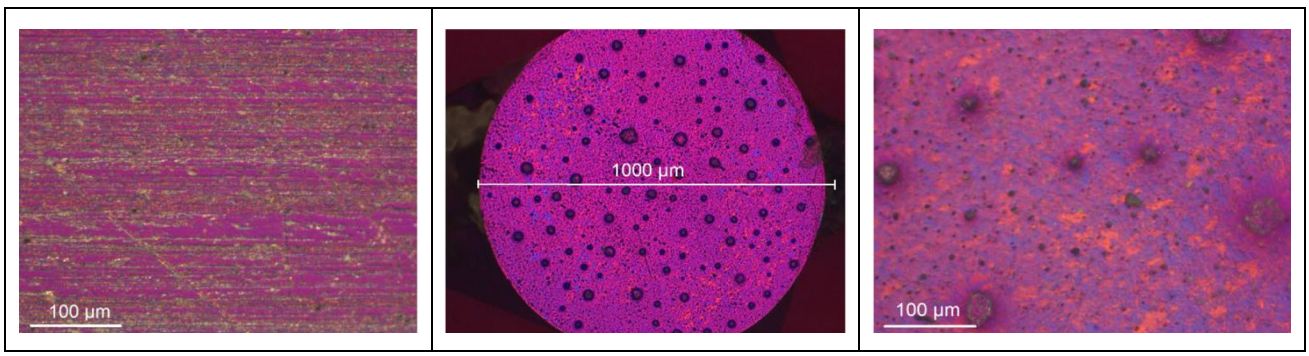

Fig. 10 Wire AlMg5. Left: longitudinal section magnification × 200; centre: cross section magnification × 25; right: cross section magnification × 200 (Barker etching)

1210.4 HM on average (30 measuring points), and 2044.8 HM in the transverse Sects. (9 measuring points).

The cuts from the build-up welding process, which can be seen in Fig. 11 (left) and Fig. 12, show a mixture of globulistic grain structures (globulites) and stem crystals, which look similar to the structural shapes in cast aluminium shown by Kuhnke [25]. A special feature is that the investigated structures from the laser cladding process grow together across the weld path boundaries. In addition, a pronounced porosity was found on all test samples after the additive deposition welding process. Its shape differs significantly from the gas pores and micro blowholes of the base material and occurs mainly on the outer and somewhat less on the inner side of the test components. A closer look (magnification × 500) clearly shows that the largest pores of 5–10 µm diameter are concentrated on the outside, especially at the layer transition in Fig. 12 (right hand side). When comparing the sections, in the additive areas without machining (component height 16–24 mm), the size of the area of the pores differs significantly. Within a 2.3 × 4 mm area (Fig. 11 left, Fig. 12), the cross-sections of the non-machined area were evaluated in terms of pore area using an image processing. The largest pore percentage of 4.51% was found for test sample B, for test sample A the value was 2.58% and for test sample C 2.25%. This correlates with the laser power in the examined component area, where the highest laser power of 1800–1680 W was applied for components group B during the application process (Fig. 3). The increase in porosity in the Al weld seam compared to the base material is, according to Goth's investigations of laser beam welding of mixed compounds of cast aluminium and wrought aluminium alloys under nitrogen, mainly due to the hydrogen absorption from oxidised and impure workpiece surfaces [26]. He demonstrated a clear correlation between the oxide layer area melted per seam volume during welding (relative oxide surface area) and the hydrogen porosity of the

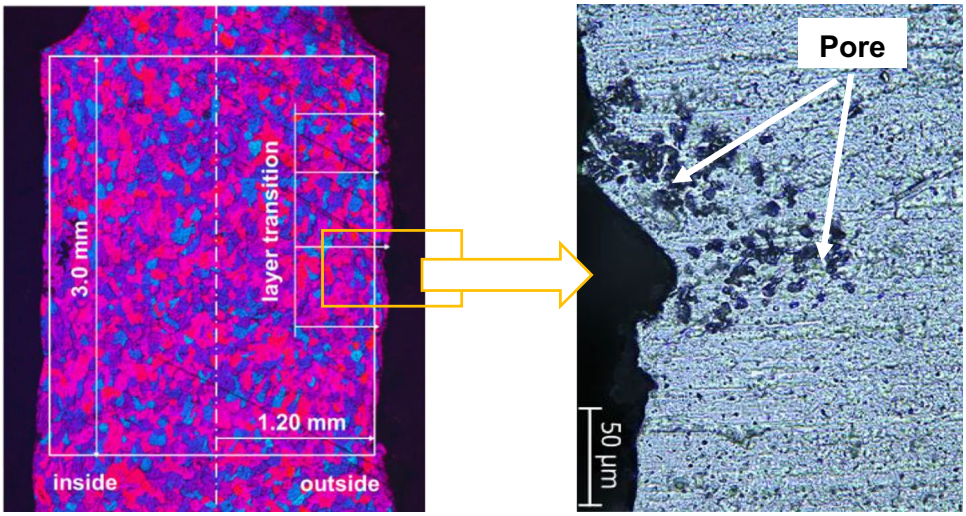

Fig. 11 Sample A: cut from additive area (cutting plane perpendicular to the printing direction). Left: magnification × 25, right: magnification × 500 (Barker-etching)

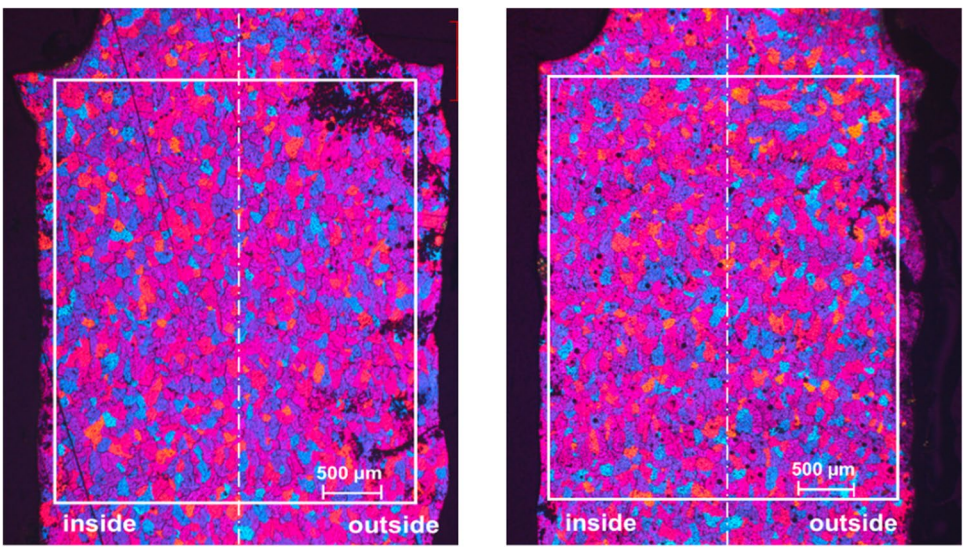

Fig. 12 Cut from additive area (cutting plane perpendicular to the printing direction). Left: sample B magnification × 500, right: sample C magnification × 500 (Barker-etching)

seam. This interpretation is highly interesting regarding the LMWD process. Further investigations with respect to this correlation are planned in future works.

Another interesting aspect is the comparison of the constituents of the microstructure of the additive manufactured component. Figure 13 shows microstructures which were taken from a tangential section of 0.16 mm depth on the outer surface of the component (Fig. 13) (and therefore parallel to the feed direction) and in the middle of the component (Fig. 14). The significantly larger individual microstructures (globulites, columnar microstructure) and microstructure agglomerations on the tangential section cut (close to the cylinder shell) in contrast to the smaller microstructures in the middle of the component can be clearly recognised. Additionally, more pores appear and combine to form larger pores at the layer transitions (Fig. 13 right). In the centre of the component in the cross-section perpendicular to the feed direction, the pores are still present, but are regularly distributed without clear localization (Fig. 14 right).

The components of the microstructure at the surface (Fig. 13 right) and in the centre of the wall of the section (Fig. 14 right) were evaluated according to the method proposed by Ohser and Lorz by means of linear analysis using spatially random quantities [27]. The points of intersection of the test lines with the grain boundaries were considered as random quantities. The test lines were placed on the measuring surface 0.489 mm × 0.401 mm. The distance between two individual vertical lines was 97.8 µm, between parallel lines 80.2 µm.

The point density P_L of the intersections was calculated according to:

$$P_L = \frac{N}{L} \tag{1}$$

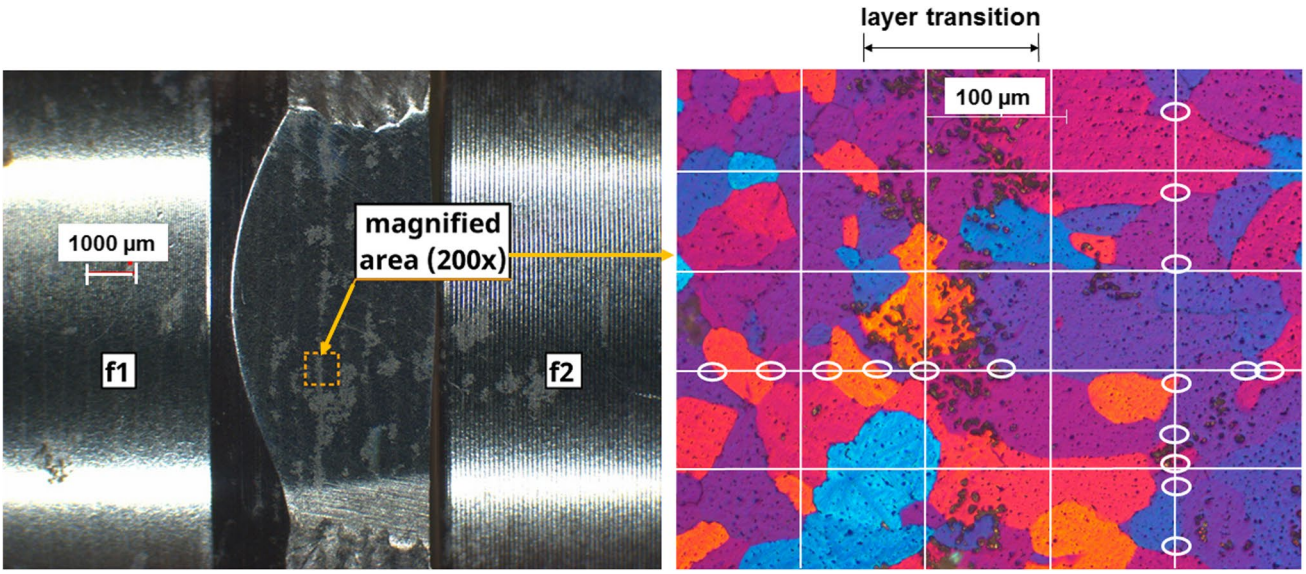

Fig. 13 Additive area, tangential section (approx. 0.16 mm depth from the outside). Measuring range in the middle, magnification × 200 with illustrative points of the intersection of test lines with the grain boundaries (sample A) (picture of a barker etching around a layer transition)

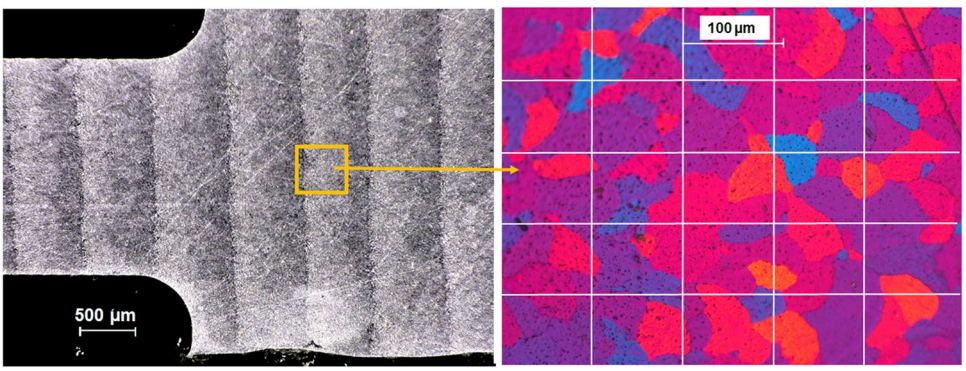

Fig. 14 Cut from additive area sample A in the middle of the wall, cutting plane perpendicular to the feed direction. Left: magnification × 25; right: magnification × 200

The test line length L is the sum of all Lx and Ly segments. N is the number of points of intersection. After the calculation, it was found that the intersection point density, and thus, the number of grains in the middle of the wall is 1.22 times higher than the intersection point density in tangential Sect. (0.16 mm from the outside wall), as can be deduced from Table 4. This indirectly indicates a smaller number of grains on the surface and a compaction of the grains in the middle of the wall. Of course, the position of the cutting plane in relation to the feed direction plays a decisive role. In Fig. 13, the cutting plane is parallel to the feed direction, while in Fig. 14, the cutting plane is perpendicular to the feed direction. This has an influence on the orientation of the microstructure.

As a further statistical analysis of the component of the microstructure on the surface and in the middle of the wall, the surface microstructure distribution was considered. For this purpose, the area of each microstructure was determined on the investigated measuring surfaces (Fig. 13 right Fig. 14 right). A comparison of the surface structure distribution shows that the centre of the component contains considerably smaller grains than the component surface. At the centre of the component, 98% of the grains have an area of $< 1.4 \times 10^5$ µm^2, at the surface $< 2.2 \times 10^5$ µm^2 (98.2% of the grains). In addition, 1.8% of the grains on the surface have an area of 2.65–3.75 $\times 10^5$ µm^2, while in the centre of the wall the grain areas do not exceed 1.95×10^5 µm^2 (Fig. 15).

Subsequently, an examination of the grains was carried out on the component areas that were post-processed (Fig. 16). It was found that the machined surfaces on both sides of the component showed a significant reduction of scorching or pores in comparison to surface areas without machining operations (Fig. 11). The porous, brittle areas were removed during machining. In addition, plastic surface deformation takes place during machining, which contributes to closing the pores through a filling effect. At the lower feed rate $f = 0.05$, this effect is more pronounced since the local contact time tool-component surface is greater and can therefore have a stronger impact on the pore structure.

Table 4 Component of the microstructure (intersection point density) of an example from group A

Cross section	Line segment length in mm	Number of intersection points	Intersection point density
A (tangential cut, section depth: 0.16 mm)	5.614	50	8.91
A (in the middle of the wall)	5.614	61	10.86

4.4 Evaluation of hardness

The microhardness was examined along the prepared microsections (Figs. 9 and 10). The hardness impressions were made in the centre of the section (cylinder wall centre). It was found that the hardness showed reduced values in the additive area without subtractive finishing (16–24 mm cylinder height) (Fig. 17). In the component areas that were reworked by turning, the hardness values for all the test samples examined tended to be 5–15% higher.

In addition, hardness degradation was observed for all components in the additive area without machining. This could be attributed to cohesive strength. Metals usually have a high cohesive strength. With increasing temperature in the LMWD process, the molecular mobility increases (Brownian molecular motions). The already quite weak secondary valence bonds dissolve with increasing temperature, and the molecular cohesion decreases [28]. Consequently, the cohesive strength also decreases with increasing temperature. This can result in a drop in hardness with component height.

To interpret the influence of the additive process, the component areas without machining were closely examined. The hardness imprints were applied specifically

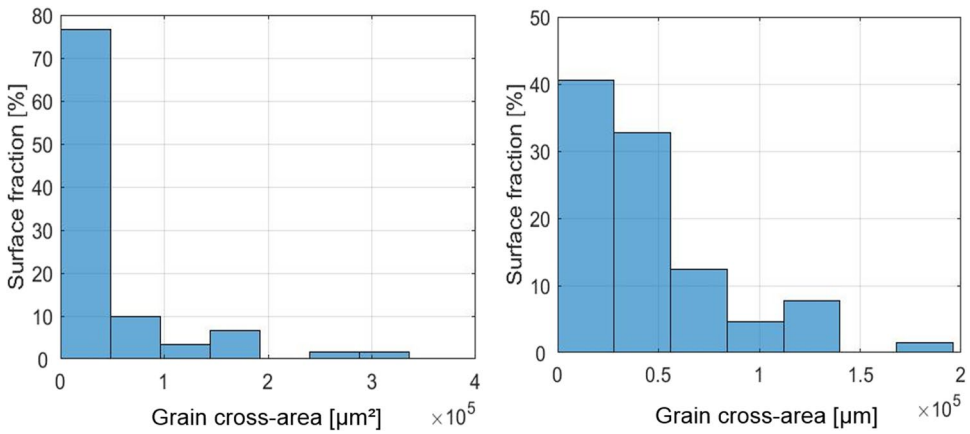

Fig. 15 Structure distribution (sample A). Left: on the surface (cut 0.16 mm depth from the outside), right: in the middle of the wall

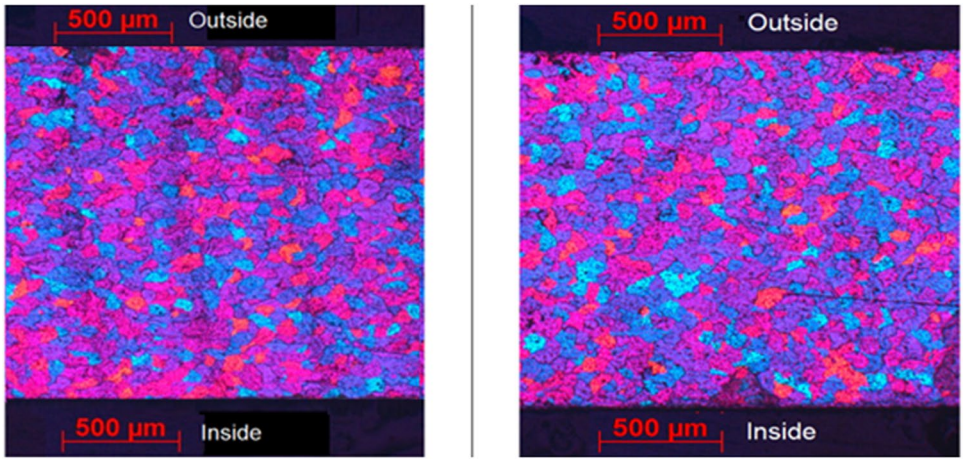

Fig. 16 Microstructure on the component sides after machining. Left: $f_1 = 0.05$; right: $f_2 = 0.1$ magnification × 25 (sample A)

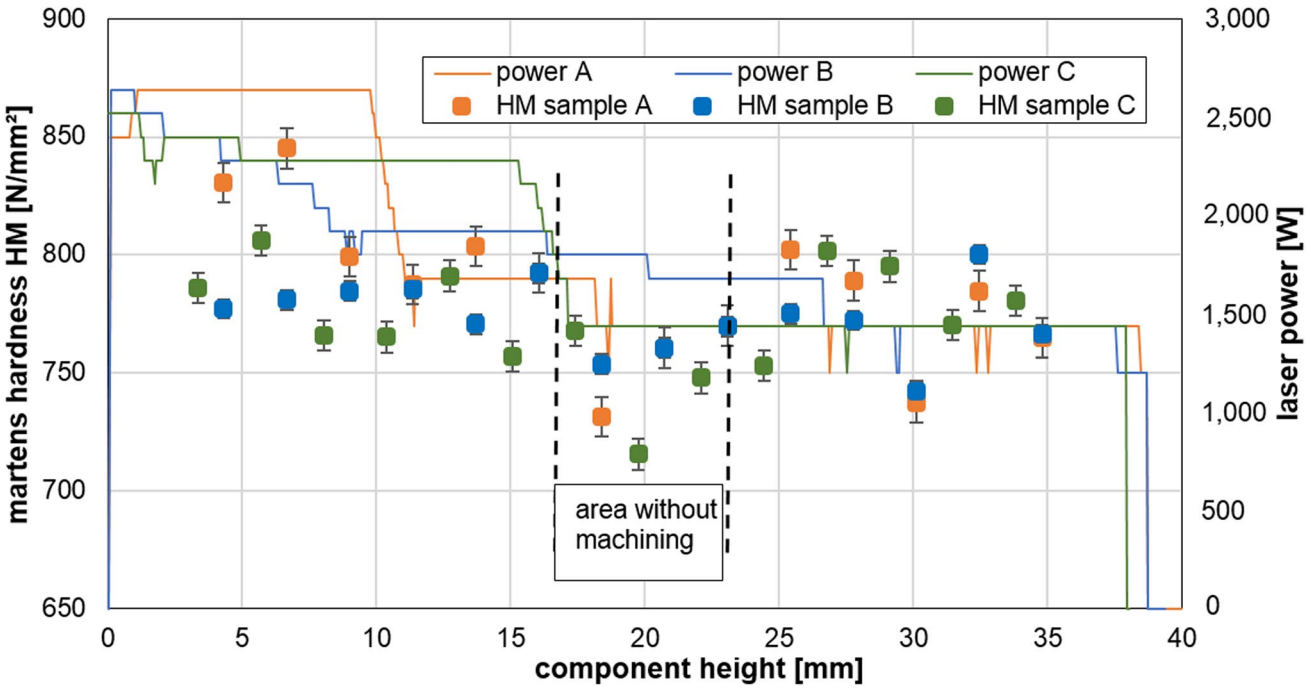

Fig. 17 Hardness progression in the centre of the component wall: cuts of samples A, B, and C. Cutting plane perpendicular to the printing direction (without top layer)

on the layer transition and inside the layer (component height 16–20 mm) and then compared with each other. In more localised hardness tests on various layers and layer boundaries, it was found that a higher laser power had a positive effect on the component hardness (Fig. 18 left). The sample B (laser power 1920–1640 W) had the highest hardness values (such as on the layer transition (741.8 N/mm^2) and inside the layers (765.05 N/mm^2)). In all tested components, the layer boundaries showed lower hardness values than the layer centres. This correlated with the observations under the light microscope in Figs. 11 and 12, where more pores appeared at the layer transitions. This corresponded to known observations when using aluminium alloy (AlMg4,5MnZr) for wire-based laser metal deposition [29]. This effect is attributed to the Mg within the alloy, since it is argued that Mg reduces the surface tension of the melt and increases the melt viscosity. This results in a reduced wettability, and the reduced wettability results in an increase of pores in the layer transitions [30], because of a bad layer-bonding behaviour. Melt gases are most probably not to blame, since the heat conductance during the process deteriorates with increasing distance from the substrate/built height. Therefore, the cooling rates become slow, and the melt has ample time for outgassing.

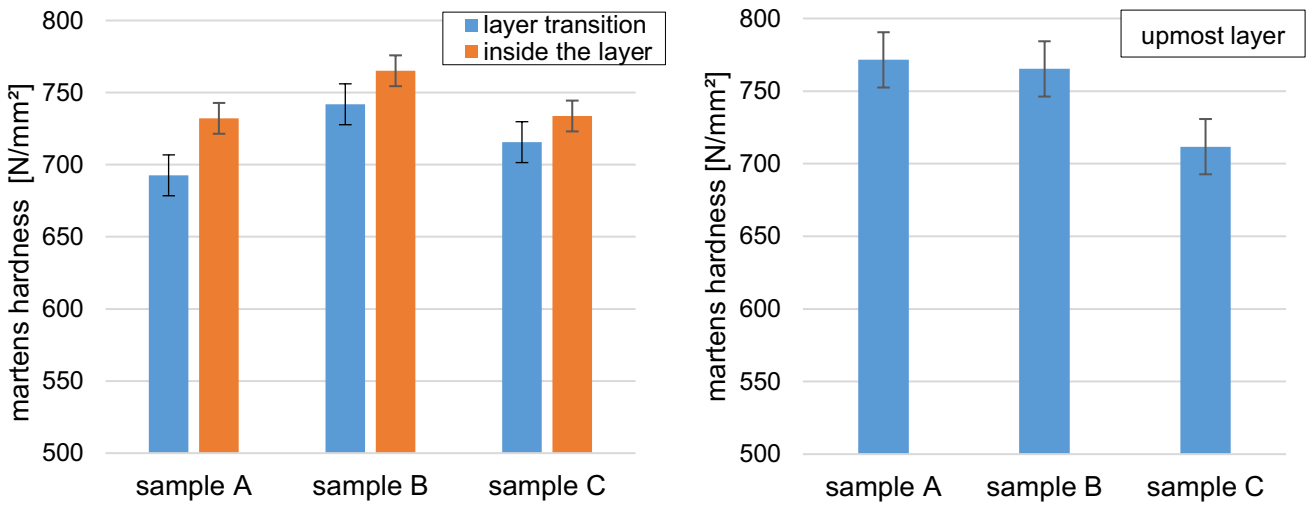

Fig. 18 Left: Hardness at the layer boundary transition and in the layer (h = 16–20 mm); right: hardness in the upmost layer. Sample A: laser power 1680–1440 W; sample B: laser power 1920–1640 W; sample C: laser power 1920–1440 W. Cutting plane perpendicular to the printing direction

Significant differences in hardness were also noticeable on the upmost layer of the test samples (Fig. 18 right). Test sample A had the highest hardness of HM 771 N/mm^2, the lowest with HM 711 N/mm^2 sample C. It was interesting to note that, after an estimation with Eqs. (2–3), the cumulative energy E1 of the laser cladding process for test sample B reached the highest value of all samples with 597.02 kJ (506.82 kJ for A and 486.08 kJ for C). However, the laser power at the end of the process (cylinder height 36–37.5 mm) was 1200 W and thus 200 W lower than A and C.

$$E_0 = \left(\sum_{i=1}^{n} P_i \Delta t\right) \tag{2}$$

$$E_1 = \left(\sum_{i=1}^{n} P_i \frac{2\pi R \Delta h_i}{d * v}\right) \tag{3}$$

where E_0 is the cumulative energy, E_1 is the cumulative energy of laser cladding process, P is the laser power in W, R is the average radius of the component in mm, Δh is the differential height of the component with specific power in mm, d is the wire diameter in mm, v is the wire speed in mm/s.

Finally, the machined area was examined at a feed rate of f = 0.1 (laser power level 1400 W for all components). For that purpose, the hardness (with a 50 µm distance from the edge) was measured on the outside and inside for component heights between 32.5 and 34.5 mm and then compared with the hardness in the centre of the wall cross-section (Fig. 19). It was found that, on the turned sides, all components had higher hardness values in comparison to the centre of the wall. The hardness after machining was higher on the component surface than in the centre of the component. The thermal effects and forces during machining led to plastic surface deformation of the surface layers. The high temperatures generally lead to a softening of the material, increased strain rates lead to a hardening. Both processes counteract each other. When machining with cooling lubricants, there is a transition from isothermal to adiabatic test conditions in the direction of the centre of the component, which leads to a heating of the sample and to thermal softening. The highest hardness values belonged to the sample B and correlated with the highest removal volumes of 96.44 mm^3 on the outside and 114.01 mm^3 on the inside of the component. In the case of removing higher material volumes, correspondingly higher temperature and cutting forces (contact pressure of the cutting edge) occurred, which resulted in a higher consolidation of the edge layers on the wall sides. For sample A, the removed volume was 60.95 mm^3 (outside) and 23.85 mm^3 (inside), C: 55 mm^3 and 31.74 mm^3 for sample C.

5 Summary

The adjustment of the laser power carried out at IFSW to suppress process overheating had a strong influence on the shape accuracy of the additive component. The experiments have shown that a stepwise adjustment of the laser power had a positive effect on the roundness and surface appearance of the additive component but could not suppress the process-related outward growth of the cylinder wall in the form of a cone. In contrast, it could be observed that a strong reduction in laser power (by about 1000 W) during the deposition process reduced the wall thickness growth rate, which

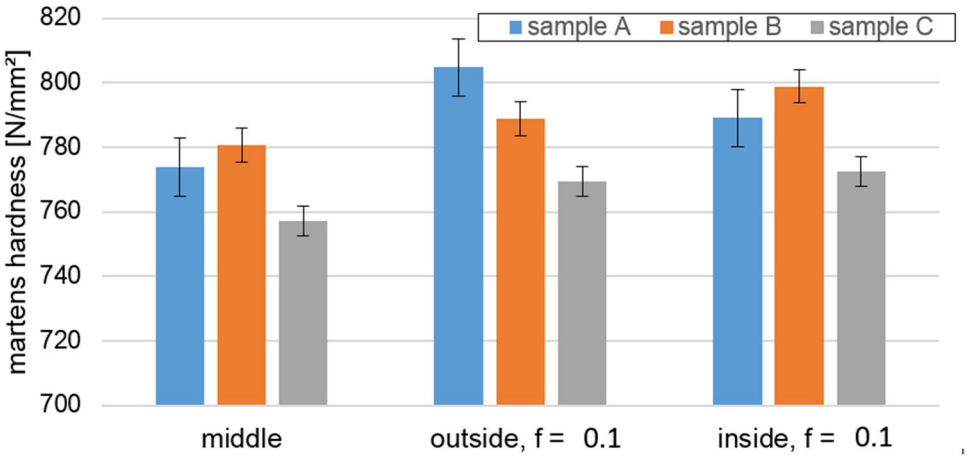

Fig. 19 Influence of machining parameters on hardness distribution in the wall cross-section. Cutting plane perpendicular to the printing direction. Machining parameters: $v_c = 500$ m/min, $f = 0.1$; measurements on height: 32.5–34.5 mm (laser power level was 1400 W for all components)

could be used to counter the aforementioned effects. However, this was also reflected in a surface inhomogeneity of the component shell.

Furthermore, it could be observed that the adjustment of the laser power influenced the height of the melting path. If the power was reduced greatly, the melting paths become higher. In addition, the wire used as a substrate in the process had hardness values that were higher by the factor of 1.61 (hardness in the longitudinal sections) than the material of the additive component after the laser deposition process (with an average hardness value of the additive samples of approx. 750 HM). If the cut of the original material transverse to the wire direction was considered, this factor even increased to 2.73. This was related to the production of the wire, which received a significant increase in hardness due to the residual compressive stresses induced by cold forming. The melting and solidification of the material eliminated these internal stresses, which is why the hardness values were significantly reduced after the additive process.

The test components produced by the LMWD process showed a good quality without the hot cracks typical for welding aluminium alloys. The porosity found in the components was mainly located on the outer surface of the component and on the layer boundaries. This showed a good agreement with other research activities in this area [29]. As a result, the hardness at the layer boundaries was lower than inside the layer.

By turning the additive components, the component quality was significantly increased. After machining, the roundness values along the height of the cylinder reached a maximum of 0.029 mm (before machining, the maximum was 0.38 mm), whereas the hardness on the machined surface ($v_c = 500$ m/min, $f = 0.1$ mm/revolution) was 3–7% higher than in the middle of component wall. This could be related to the volume of the removed material, which had a significant influence on the component hardness near the surface. Due to the shape inhomogeneity of the LMWD test components, different hardness values were found along the component sides after machining. A higher machining volume could result in locally higher hardness values.

In future investigations, the LMWD process with subsequent machining will be further investigated. The aim will be to produce components with a high accuracy and defined values of hardness in the additive-subtractive manufacturing process.

Acknowledgements The authors would like to thank the Baden-Württemberg Ministry of Science, Research and Arts for the financial support of the projects within the *InnovationsCampus Mobilität der Zukunft*.

Author contribution H.-C. Möhring elaborated the concept of the study. D. Becker and T. Reeber performed and analysed the experimental investigations with the support of R. Eisseler. D. Becker wrote the manuscript in consultation with H.-C. Möhring. T. Stehle participated in the design of the study and its coordination.

Funding Open Access funding enabled and organized by Projekt DEAL. Open Access funding provided by the University of Stuttgart and project funding by the Baden-Württemberg Ministry of Science, Research within the InnovationsCampus Mobilität der Zukunft.

Data availability The paper has no associated software. All data gathered regarding this publication is presented.

Code availability Not applicable.

Declarations

Ethical approval All procedures performed in studies involving human participants were in accordance with the ethical standards of the institutional and/or national research committee and with the 1964 Helsinki declaration and its later amendments or comparable ethical standards.

Consent to participate Informed consent was obtained from all individual participants included in the study.

Consent for publication The participant has consented to the submission of the case report to the journal.

Conflict of interest The authors declare no competing interests.

References

1. Bolat Ç, Akgün İC, Göksenli A (2020) On the way to real applications: aluminum matrix syntactic foams. Eur Mech Sci 4(3):131–141. https://doi.org/10.26701/ems.703619
2. Hovorun TP, Berladir KV, Pererva VI, Rudenko SG, Martynov AI (2017) Modern materials for automotive industry. JES 4(2):f8–f18. https://doi.org/10.21272/jes.2017.4(2).f8
3. Ribes H (2019) Aluminum applications in lightweight design for small commercial vehicles and station wagons. ATZ Prod Worldw 6(1):42–45. https://doi.org/10.1007/s38312-019-0004-0
4. Stojanovic B, Bukvic M, Epler I (2018) Application of aluminum and aluminum alloys in engineering. Appl Eng Lett 3(2):52–62. https://doi.org/10.18485/aeletters.2018.3.2.2
5. Wesolowski K (2009) Leichtbau unter Anwendung der Aluminium-Sandwichtechnik. Lightweight Des 2(4–5):46–50. https://doi.org/10.1007/BF03223578
6. DebRoy T, Wei HL, Zuback JS, Mukherjee T, Elmer JW, Milewski JO, Beese AM, Wilson-Heid A, De A, Zhang W (2018) Additive manufacturing of metallic components – Process, structure and properties. Prog Mater Sci 92:112–224. https://doi.org/10.1016/j.pmatsci.2017.10.001
7. Karakurt I, Lin L (2020) 3D printing technologies: techniques, materials, and post-processing. Curr Op Chem Eng 28:134–143. https://doi.org/10.1016/j.coche.2020.04.001
8. Wang Z, Ummethala R, Singh N, Tang S, Suryanarayana C, Eckert J, Prashanth KG (2020) Selective laser melting of aluminum and its alloys. Materials (Basel) 13(20):4564. https://doi.org/10.3390/ma13204564
9. Möhring H-C, Stehle T, Becker D, Eisseler R (2018) Qualität von additiv hergestellten PLA-Bauteilen. wt Werkstattstechnik online 108(6):419–425
10. Ding D, Pan Z, Cuiuri D, Li H (2015) Wire-feed additive manufacturing of metal components: technologies, developments and future interests. Int J Adv Manuf Technol 81(1–4):465–481. https://doi.org/10.1007/s00170-015-7077-3
11. Fuchs C, Baier D, Semm T, Zaeh MF (2020) Determining the machining allowance for WAAM parts. Prod Eng Res Devel 14(5–6):629–637. https://doi.org/10.1007/s11740-020-00982-9
12. Bai Y, Chaudhari A, Wang H (2020) Investigation on the microstructure and machinability of ASTM A131 steel manufactured by directed energy deposition. J Mater Process Technol 276:116410. https://doi.org/10.1016/j.jmatprotec.2019.116410
13. Bai Y, Zhao C, Yang J, Hong R, Weng C, Wang H (2021) Microstructure and machinability of selective laser melted high-strength maraging steel with heat treatment. J Mater Process Technol 288:116906. https://doi.org/10.1016/j.jmatprotec.2020.116906
14. Chernovol N, Sharma A, Tjahjowidodo T, Lauwers B, van Rymenant P (2021) Machinability of wire and arc additive manufactured components. CIRP J Manuf Sci Technol 35:379–389. https://doi.org/10.1016/j.cirpj.2021.06.022
15. Oyelola O, Crawforth P, M'Saoubi R, Clare AT (2018) On the machinability of directed energy deposited Ti6Al4V. Addit Manuf 19:39–50. https://doi.org/10.1016/j.addma.2017.11.005
16. Oyelola O, Jackson-Crisp A, Crawforth P, Pieris DM, Smith RJ, M'Saoubi R, Clare AT (2020) Machining of directed energy deposited Ti6Al4V using adaptive control. J Manuf Process 54:240–250. https://doi.org/10.1016/j.jmapro.2020.03.004
17. Syed WUH, Li L (2005) Effects of wire feeding direction and location in multiple layer diode laser direct metal deposition. Appl Surf Sci 248(1–4):518–524. https://doi.org/10.1016/j.apsusc.2005.03.039
18. Williams SW, Martina F, Addison AC, Ding J, Pardal G, Colegrove P (2016) Wire + arc additive manufacturing. Mat Sci Technol 32(7):641–647. https://doi.org/10.1179/1743284715Y.0000000073
19. Syed WUH, Pinkerton AJ, Li L (2005) A comparative study of wire feeding and powder feeding in direct diode laser deposition for rapid prototyping. Appl Surf Sci 247(1–4):268–276. https://doi.org/10.1016/j.apsusc.2005.01.138
20. Abioye TE, Folkes J, Clare AT (2013) A parametric study of Inconel 625 wire laser deposition. Mat Proc Technol 213(12):2145–2151. https://doi.org/10.1016/j.jmatprotec.2013.06.007
21. Becker D, Boley S, Eisseler R, Stehle T, Möhring H-C, Onuseit V, Hoßfeld M, Graf T (2021) Influence of a closed-loop controlled laser metal wire deposition process of S Al 5356 on the quality of manufactured parts before and after subsequent machining. Prod Eng Res Devel. https://doi.org/10.1007/s11740-021-01030-w
22. Ingersoll Cutting Tools Marketing- & Technologie-Standort Deutschland Ingersoll Werkzeuge GmbH (2017) Technisches Handbuch Drehen, Stechen & Gewindedrehen 2017. https://www.ingersoll-imc.de/fileadmin/user_upload/user_upload/pdfs/Handbuecher/THB_Fraesen_02_2017.pdf. Accessed 19 Dec 2020
23. Kostron H (1952) Aluminium und Gas. 2. Blasen und Poren im Knetmaterial. Zeitschrift für Metallkunde 43(11):373–387
24. Lutze P, Ruge J (1990) Wasserstoff in Aluminium und seinen Legierungen. Metall Wirtschaft, Wissenschaft und Technik 44:741–748
25. Kuhnke K (2012) Aluminium, was nun? https://www.gmr2.de/uploads/bilder/Alu.pdf. Accessed 27 Feb 2021
26. Goth KT (2004) Schweißen von Mischverbindungen aus Aluminiumguß- und Knetlegierungen mit CO2-Laser unter besonderer Berücksichtigung der Nahtart. Zugl.: Stuttgart, Univ., Diss., 2004. Laser in der Materialbearbeitung - Forschungsberichte des IFSW. Utz, München
27. Ohser J, Lorz U (1994) Quantitative Gefügeanalyse: Theoretische Grundlagen und Anwendung; mit Tabellen, 1. Aufl. Freiberger Forschungshefte B Metallurgie und Werkstofftechnik, Werkstoffeinsatz, vol 276. Dt. Verl. für Grundstoffindustrie, Leipzig, Stuttgart

28. Schulze G (2010) Die Metallurgie des Schweissens: Eisenwerkstoffe - nichteisenmetallische Werkstoffe, 4., neu bearbeitete Aufl. VDI-Buch. Springer, Heidelberg, New York
29. Froend M, Riekehr S, Kashaev N, Klusemann B, Enz J (2018) Process development for wire-based laser metal deposition of 5087 aluminium alloy by using fibre laser. J Manuf Process 34:721–732. https://doi.org/10.1016/j.jmapro.2018.06.033
30. Ding Y, Muñiz-Lerma JA, Trask M, Chou S, Walker A, Brochu M (2016) Microstructure and mechanical property considerations in additive manufacturing of aluminum alloys. MRS Bull 41(10):745–751. https://doi.org/10.1557/mrs.2016.214